Metal and Ligand Effects on Coordinated Methane pK_a. Direct Correlation with the Methane Activation Barrier

Amy S. Guan, Ivy X. Liang, Christopher X. Zhou, Thomas R. Cundari

Department of Chemistry
Center for Advanced Scientific Computing and Modeling (CASCaM)

University of North Texas

Abstract: DFT and coupled cluster methods were used to investigate the impact of 3d metals and ligands upon the acidity and activation of coordinated methane C–H bonds. A strong, direct relationship was established between the pK_a of coordinated methane and the subsequent free energy barriers to H_3C–H activation. The few outliers to this relationship indicated other factors– such as thermodynamic stability of the product and ligand-metal coordination type – also impacted the methane activation barrier ($\Delta G^{\ddagger}$). High variations in the activation barriers and pK_a values were found with a range of 34.8 kcal/mol for the former and 28.6 pK_a units for the latter. Clear trends among specific metals and ligands were also derived; specific metals, such as Co^{I}, as well as Lewis and π-acids consistently yielded higher acidity for the ligated methane and hence lower $\Delta G^{\ddagger}$.

Introduction

Methane is an abundant hydrocarbon and the primary component of natural gas, which has led to methane functionalization being an intense field of study in energy research.[1,2,3] The process of methane functionalization has a wide range of industrial applications, including the conversion of methane to methanol, a liquid fuel that can provide a cleaner source of energy than traditional fossil fuels and act as a chemical feedstock in place of petroleum.[1,2] Methanol retains much of the energetic properties of methane and, being a liquid, has the added benefit of being much more efficient to transport.[1,3] However, because methane is highly unreactive, the selective conversion of methane to methanol is impractical without the aid of catalysts.[1,2]

A study by Olah and Schlosberg[4] indicated that methane, which is typically a very stable hydrocarbon, is only readily protonated under extreme conditions using superacids. Similarly, a study by Streitwieser and Taylor[5] suggested that methane is an extremely poor Brønsted-Lowry acid, except in the presence of superbases. However, superacidic and superbasic solutions involve impractical, extreme conditions, and highly reactive reagents that are typically characterized by stoichiometric rather than catalytic reactivity. Transition metal catalysis poses an alternative catalytic approach to methane functionalization that occurs under milder conditions and with higher selectivity.[2,6]

One method to increase the favorability of methane activation involves studying how various transition metals and supporting ligands impact the pK_a of a ligated methane C–H bond and hence facilitate its eventual activation. Previous studies have shown the significance of pK_a in promoting bond activation.[7,8] In the field of biocatalysis, Pitsawong *et al*.[7] investigated the use of flavin-dependent mono-oxygenases to catalyze phenol oxidation. Their study found that the binding of the monooxygenase to the phenol reduced its acidity by 1.6 to 2.5 pK_a units, based on protein type, thus enhancing the catalysis. These results highlight the importance of substrate acid/base properties in biocatalysis. The obvious challenge for methane activation is the much more pronounced requirement for pK_a reduction of the C–H bond prior to activation. In a rare computational study of the pK_a(C–H) of methane coordinated to "naked," monovalent 3d metal ions by Zhou and Cundari,[8] it was demonstrated that the metal ion has a substantial impact on increasing the C–H bond acidity of methane; metal identity provided a significant difference in calculated ΔpK_a(C–H) ranging from 8 to 36 pK_a units.

While previous reports have focused on the pK_a(C–H) of organic acids,[9] studies on the pK_a of C–H bonds in hydrocarbons that are coordinated to metals are rare.[8] This area of chemistry has been understudied largely due to the traditional experimental limitations of measuring pK_a for very weak hydrocarbon acids, despite the importance of pK_a in determining catalytic potential.[10] Furthermore, little is known about the possible correlation of pK_a(C–H) with C–H activation barriers. For these reasons, the present computational study was initiated.

Building off the conclusions derived from the study by Zhou and Cundari,[8] this research examined the coordination of methane to complexes comprised of 3d metals (M = Fe^{I}, Co^{I}, Ni^{I}, Cu^{I}) and coordinated neutral supporting ligands (L = AlH_3, BH_3, CNH, CO, NCH, OH_2, NH_3, PH_3, SH_2) of differing donor/acceptor properties. Theory was used to determine the effect of metal and ligand identity on the acidity of coordinated methane, and the subsequent favorability of methane deprotonation. A Brønsted-Lowry acid-base reaction was investigated for methane activation. The reaction involved a transition metal-methane adduct of the form $[L\text{-}M\cdots CH_4]^+$ (**Figure 1**) reacting with the Lewis base NH_3 in a continuum solvent dimethyl sulfoxide (DMSO). All 3d metal ions were assumed to have a formal oxidation state of 1+ to facilitate comparisons among them. Likewise, all studied ligands are formally neutral. In the reaction of interest, **Figure 1**, methane is loosely coordinated to the metal cation. During the transition state (TS), a formal proton transfer occurs, activating the methane and producing ammonium. As the reaction proceeds to completion, the bond between the methane and the metal ion is strengthened by the transfer of electrons from the C–H bond to the metal-methyl bond. Thus, a neutral methyl complex is produced, $[L\text{-}M\text{–}CH_3]$, which is the conjugate base of the cationic methane adduct.

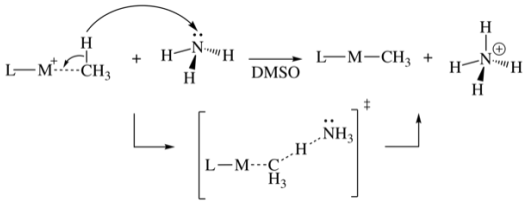

Figure 1. Acid-base reaction used to obtain the free energy barriers, free energy changes, and pK_a values relevant to methane activation: a cationic ligand-metal methane adduct and an ammonia molecule, in SMD-DMSO continuum solvent, react, which results in a ligand-metal-methyl complex and an ammonium ion.

Methodology

All geometries in this study were optimized at the B3LYP/6-31+G(d)/SMD-DMSO level of theory within the Gaussian16[11] software package. Vibrational frequencies were computed to assure the appropriate number of imaginary frequencies, as well as obtain the enthalpic and entropic corrections needed for free energy calculations. Single point energies were calculated at the optimized geometries using the ORCA[12,13] code (version 4.2.1), by employing the DLPNO-CCSD(T) technique in conjunction with the def2-QZVPP basis set. The basis set choice was derived from a previous report,[4] which indicated that quadruple-zeta basis sets provided an accuracy comparable to that of quintuple-zeta basis sets with lower expense. Their methodology, as in the present research, utilized the SMD continuum solvent model to simulate a DMSO solution.

For the reaction modeled of the form $[L\text{-}M\cdots CH_4]^+ + NH_3 \rightarrow [L\text{-}M\text{–}CH_3] + NH_4^+$, **Figure 1**, data consisting of single point energy and DFT-computed thermal correction to the Gibbs free energy for the reactants , transition state, and products were used to compute the pK_a, Gibbs free energy of deprotonation (ΔG), and Gibbs free energy barrier ($\Delta G^{\ddagger}$, methane activation barrier) for each reaction. Initial pK_a values were computed using the equation, pK_a calc. =

$\frac{\Delta G}{2.303 \cdot RT}$. Then, the following linear correction derived from the work of Nazemi and Cundari[14] was applied to the calculated pK_a value:

$$\text{p}K_a \text{ est.} = (1.0308 \cdot \text{p}K_a \text{ calc.}) - 12.146$$

to obtain the final estimated pK_a(C–H) of the methane adduct, $[\text{L-M}^{\cdots}\text{CH}_4]^+$.

Results and Discussion

The predicted ground state multiplicities of the ligand-3d metal methane adducts (**Table S1**) agreed with the lowest energy multiplicities proposed in a study that modeled methane adducts of 3d ions in the absence of any supporting ligands.[8] One exception was the Fe^I ion, where DLPNO-CCSD(T)/def2-QZVPP/SMD-DMSO (hereafter CCSD(T)) calculations predicted a quartet ground state for all $[\text{LFe}^{+\cdots}\text{CH}_4]$, whereas Zhou and Cundari[8] predicted a sextet ground state for $[\text{Fe}^{+\cdots}\text{CH}_4]$. While the quartet was consistently shown to provide a lower energy ground state, the difference in energy between the quartet and sextet states was small, with the former being lower by only a few kcal/mol. The CCSD(T) calculations indicated that the quartet state was more favorable for the Fe^I methane adducts. A second caveat was the case of the Mn^I ion, where CCSD(T) calculations predicted a combination of quintet and septet ground states for $[\text{LMn}^{+\cdots}\text{CH}_4]$ while Zhou and Cundari[8] predicted a septet ground state for the naked Mn^I ion. The possible discrepancy is similar to that of Fe^I, in which certain ground spin states predicted by DFT and CCSD(T) did not align.

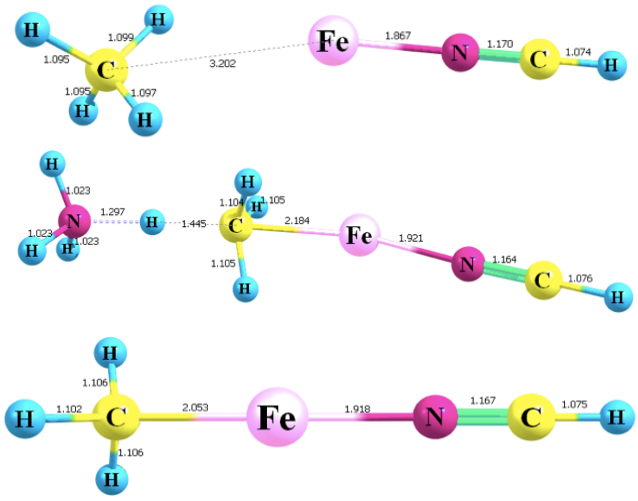

Figure 2. B3LYP/6-31+G(d)/SMD-DMSO optimized HCN-Fe^+ complexes (HCN-Fe^I-methane adduct, **top**; HCN-Fe^I transition state for methane activation by ammonia, **middle**; the conjugate base, HCN-Fe^I-methyl complex, **bottom**) as representative examples of geometries obtained for stationary points modeled in this study. Bond lengths in Å.

In **Table 1** and **Table 2**, using the DLPNO/def2-QZVPP/SMD-DMSO//B3LYP/6-31+G(d)/SMD-DMSO level of theory, the free energy barriers for methane activation and the estimated pK_a(C–H) values were computed and are displayed for each ligand-metal pair. The corresponding free energies for the overall reaction from which pK_a(C–H) values were derived are summarized in Supporting Information. **Figure 3** and **Figure 4** show the free energy barriers computed for the different L/M combinations studied.

In general, lower free energy barriers were calculated for the Lewis acids, AlH_3 and BH_3, and the π-acid CO. The highest $\Delta G^{\ddagger}$ were obtained for Lewis bases such as NH_3 and OH_2, **Figure 3**. The Lewis acid AlH_3 yielded the lowest average free energy barrier of 17.7 ± 4.8 kcal/mol among all ligands tested and the lowest free energy barrier for each metal except for AlH_3-Cu^+ and AlH_3-Mn^+, for which AlH_3 provided the fourth and third lowest $\Delta G^{\ddagger}$ of all ligands, respectively, **Table 3** AlH_3 consistently provided the lowest pK_a values for each of the metals modeled herein, **Figure 5.**

The LCo^I complexes consistently provided the lowest methane activation barrier for each ligand among all five metals tested except in the case of BH_3-Mn^I, **Figure 4**. Thus, the LCo^I complexes yielded the lowest average free energy barrier of 19.5 ± 4.4 kcal/mol among all five metals tested, **Table 4**. However, despite this generally strong consistency, LCo^I complexes did not always result in the lowest pK_a value for each ligand among the other LM^+ complexes, **Figure 6**. The LNi^I complexes generally had the highest methane activation barriers and pK_a values except compared to some of the Lewis base ligand pairings with Mn^I, **Figure 4** and **Figure 6**.

Table 1. Free energy barriers (kcal/mol) for methane activation by ammonia for 3d $[\text{LM}^{\cdots}\text{CH}_4]^+$ adducts computed at the DLPNO/def2-QZVPP/SMD-DMSO//B3LYP/6-31+G(d)/SMD-DMSO level of theory.

L	Mn^I	Fe^I	Co^I	Ni^I	Cu^I
AlH_3	20.2	13.4	12.1	19.4	23.4
BH_3	15.6	18.0	17.6	24.8	33.7
HNC	21.2	22.4	20.5	30.2	21.9
CO	19.4	17.2	13.7	25.7	19.9
HCN	20.0	21.3	20.1	31.1	20.9
NH_3	36.4	32.8	26.1	36.1	26.1
H_2O	28.2	29.6	22.0	31.1	25.0
PH_3	46.9	25.5	20.6	31.5	25.6
SH_2	33.2	25.7	23.2	30.1	25.2

Table 2. Estimated pK_a values of ligand-3d metal methane adducts computed from the ΔG values in Table S-2. Calculated at the DLPNO/def2-QZVPP/SMD-DMSO//B3LYP/6-31+G(d)/SMD-DMSO level of theory.

L	Mn^I	Fe^I	Co^I	Ni^I	Cu^I
AlH_3	-21.8	-18.0	-21.6	-14.0	-18.2
BH_3	-20.3	-14.0	-14.0	-9.8	-10.1
HNC	-13.0	-9.0	-11.5	-4.7	-10.5
CO	-11.4	-14.3	-17.0	-9.3	-15.0
HCN	-15.4	-12.8	-10.9	-2.9	-12.4
NH_3	3.9	-0.6	-6.8	2.2	-7.3
H_2O	6.8	-6.8	-9.5	-3.2	-11.6
PH_3	2.2	-8.8	-10.4	-4.2	-9.1
SH_2	0.9	-3.5	-8.8	-4.7	-10.2

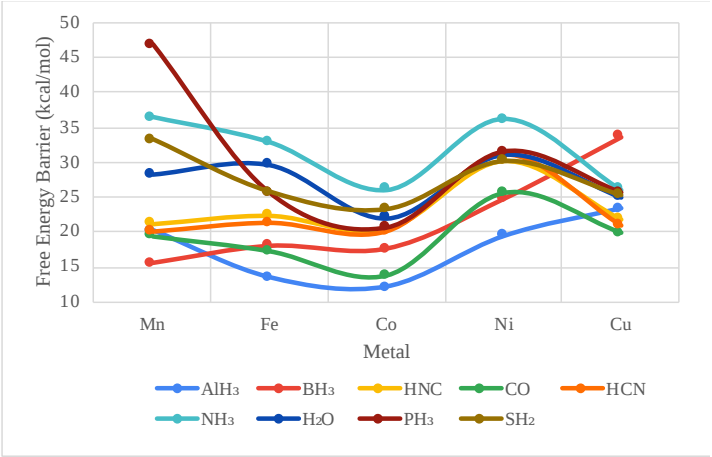

Figure 3. DLPNO/def2-QZVPP/SMD-DMSO//B3LYP/6-31+G(d)/SMD-DMSO calculated free energy barriers (kcal/mol) for methane activation for the various ligand-metal complexes organized by metal.

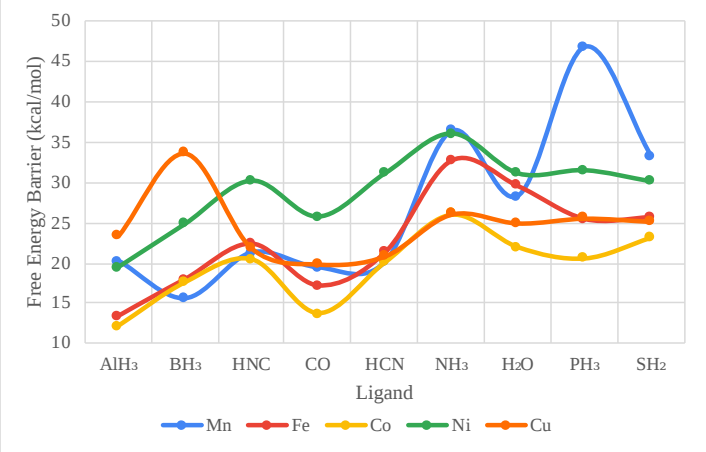

Figure 4. DLPNO/def2-QZVPP/SMD-DMSO//B3LYP/6-31+G(d)/SMD-DMSO calculated free energy barriers (kcal/mol) for methane activation among the ligand-metal complexes organized by ligand.

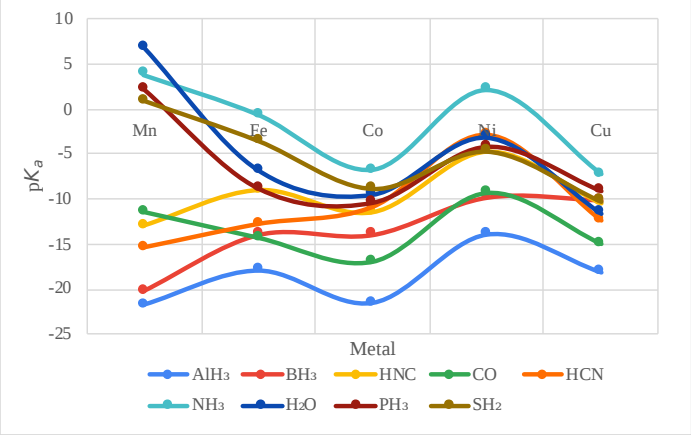

Figure 5. DLPNO/def2-QZVPP/SMD-DMSO//B3LYP/6-31+G(d)/SMD-DMSO calculated pK_a(C–H) trends for the various ligand-metal methane adducts organized by metal.

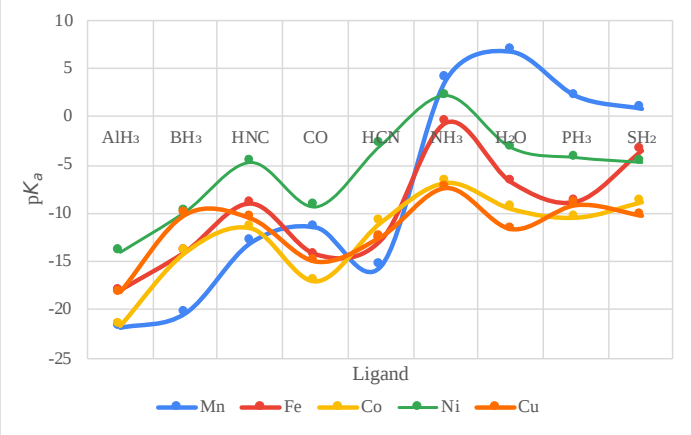

Figure 6. DLPNO/def2-QZVPP/SMD-DMSO//B3LYP/6-31+G(d)/SMD-DMSO calculated pK_a(C–H) trends among the various ligand-metal methane adducts organized by ligand.

Table 3 organizes the average and standard deviations for the $\Delta G^{\ddagger}$ and the estimated pK_a values for the ligand-3d metal methane adducts by metal. **Table 4** organizes the same averages and standard deviations by ligand. The results indicated that LCo^{I} yielded the lowest average $\Delta G^{\ddagger}$ of 19.5 kcal/mol and lowest average methane pK_a of -12.3 pK_a units. LCu^{I} yielded the lowest standard deviation in calculated $\Delta G^{\ddagger}$, ±2.2 kcal/mol, and pK_a, ±4.0 pK_a units. Hence, the results suggest that the d^{10}-CuL^{+} complexes showed the least sensitivity to ligand modification; it is hypothesized that this may be a reflection of the closed-shell nature of the Cu^{I} ion. The results further indicated that AlH_3 yielded the lowest average $\Delta G^{\ddagger}$ of 17.1 kcal/mol and lowest average pK_a of -18.7 pK_a units. The OH_2 ligand yielded the smallest standard deviation in $\Delta G^{\ddagger}$, ±3.7 kcal/mol, and the CO ligand yielded the smallest standard deviation in pK_a, ±3.0 pK_a units. Taken together, these data suggest a correlation between pK_a(C–H) values for ligated methane and its subsequent activation barrier.

Table 3. Average and standard deviations of calculated properties (free energy barriers (kcal/mol) and pK_a (pK_a units)) of ligand-3d metal adducts for each ligand. Calculated at the DLPNO/def2-QZVPP/SMD-DMSO//B3LYP/6-31+G(d)/SMD-DMSO level of theory.

	AlH_3	BH_3	CNH	CO	NCH	NH_3	OH_2	PH_3	SH_2
$\Delta G^{\ddagger}$, ave.	17.7	21.9	23.2	19.2	22.7	31.5	27.2	30.0	27.5
$\Delta G^{\ddagger}$, stdev.	4.8	7.4	4.0	4.4	4.7	5.1	3.7	10.2	4.1
pK_a est., ave.	-18.7	-13.6	-9.7	-13.4	-10.9	-1.7	-4.9	-6.1	-5.3
pK_a est., stdev.	3.2	4.2	3.2	3.0	4.7	5.1	7.2	5.2	4.4

Table 4. Average and standard deviations of calculated properties (free energy barriers (kcal/mol) and pK_a (pK_a units)) of ligand-3d metal adducts for each metal. Calculated at the DLPNO/def2-QZVPP/SMD-DMSO//B3LYP/6-31+G(d)/SMD-DMSO level of theory.

	Mn^{I}	Fe^{I}	Co^{I}	Ni^{I}	Cu^{I}
$\Delta G^{\ddagger}$ ave.	26.8	22.9	19.5	28.9	24.6
$\Delta G^{\ddagger}$ std. dev.	10.2	6.2	4.4	4.9	4.0
pK_a-est. ave.	-7.6	-9.8	-12.3	-5.6	-11.6
pK_a-est. std. dev.	11.0	5.6	4.6	4.7	3.3

Figure 7 indicates that the free energy barrier of the methane deprotonation and the pK_a of the reaction have a positive, linear correlation (R^2 = 0.75). Five outliers were found: AlH_3-Cu^{I}, BH_3-Cu^{I}, AlH_3-Cu^{I}, H_2O-Mn^{I}, and PH_3-Mn^{I}, denoted by red dots in **Figure 7**. All of the outliers involved copper or manganese among the metals, and the majority involved Lewis acid supporting ligands, AlH_3 or BH_3.

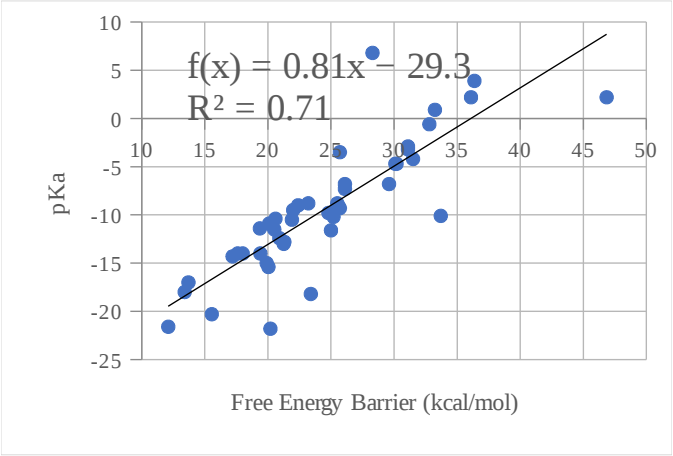

Figure 7. The relationship between free energy barrier and pK_a is illustrated using a linear regression. Five outliers (red) include AlH_3-Cu^{I}, BH_3-Cu^{I}, AlH_3-Cu^{I}, and PH_3-Mn^{I} below the line of best fit and H_2O-Mn^{I} above the line of best fit. With these five outliers excluded, the R^2 value is 0.91.

Figures 8 - 10 depict the geometries of the BH_3-Cu^{I} methane complexes whose values are an outlier in the graph of the relationship between free energy barrier and pK_a, **Figure 7**. A single geometry was found for the BH_3-Cu^{I} methane adduct, **Figure 8**, but two isomers were found for the transition state, **Figure 9**, and the BH_3-Cu^{I} methyl conjugate base, **Figure 10**. The BH_3-Cu^{I} conjugate base is interesting in that it involves a short, covalent B–C bond length (1.63 Å), suggesting this as the product of a subsequent functionalization (C–X bond forming) step in the catalytic cycle after initial C–H activation of methane. Similar considerations apply to the H_3Al-Cu^{I} outlier.

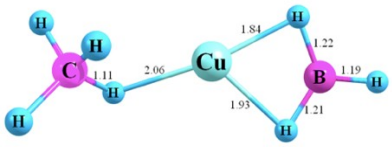

Figure 8. DFT-optimized structure of the BH_3-Cu^I methane adduct.

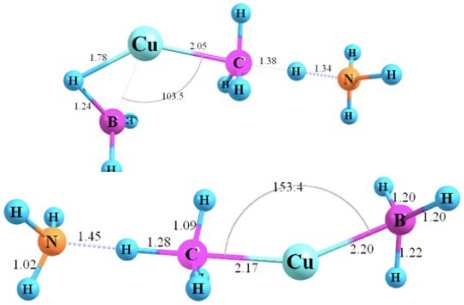

Figure 9. Two isomers were isolated for the BH_3-Cu^I transition state for methane activation by ammonia. The more stable isomer (**top**) exhibits a bent geometry with a 103.5° C-Cu-B bond and an activation barrier of 33.7 kcal/mol. The less stable isomer (**bottom**) has a more linear geometry with a 153.5° C-Cu-B bond and an activation barrier of 42.7 kcal/mol.

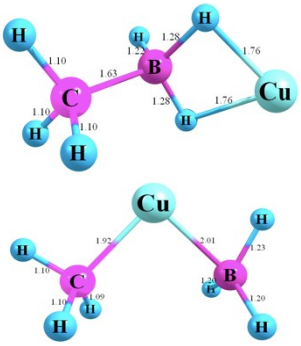

Figure 10. Two isomers of the BH_3-Cu^I methyl complex that were identified by DFT optimization. The more stable isomer (**top**) is that resulting from a later stage (functionalization) of the reaction with a covalent B–C bond with a free energy change of -2.7 kcal/mol and a pK_a of -27.0. In the less stable isomer (**bottom**), the borane and the methyl group are both coordinated to Cu without formation of a B–C bond (distance ~ 2.7 Å) with a free energy change of 2.7 kcal/mol and a pK_a(C–H) of -10.1.

Figure 11 depicts the C–H activation transition state geometries for H_2O-Mn^I models, whose values are an outlier in the graph of the relationship between free energy barrier and pK_a, **Figure 7**. The transition states exhibited different coordination between ligand and metal, which likely contributed to contrasting predictions of lowest energy spin state between B3LYP/6-31+G(d)/SMD-DMSO calculation (which predicted a quintet spin state) and DLPNO-CCSD(T)/def2-QZVPP/SMD-DMSO (which predicted a septet).

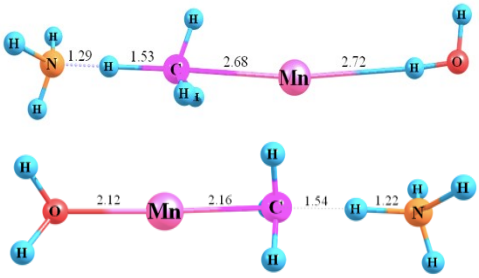

Figure 11. Septet (**top**) and quintet (**bottom**) geometries of the H_2O-Mn^I transition state for methane activation by ammonia. B3LYP/6-31+G(d)/SMD-DMSO calculations predicted the septet TS to be more stable, being lower in energy by ~12.0 kcal/mol. By contrast, single-point calculations at the DFT-optimized geometry with the DLPNO-CCSD(T)/def2-QZVPP/SMD-DMSO technique indicated that the quintet TS is the most energetically favorable structure, ~12.2 kcal/mol lower in energy. The binding of H_2O in the septet TS occurs through outer sphere binding while the binding mode for the quintet TS occurs through the inner coordination sphere. The largest PNO amplitudes were < 0.1 for the septet TS and ~ 0.14 for the quintet TS.

Summary and Conclusions

The goal of this research was to examine how the combination of supporting ligands and metal identity in simple organometallic complexes can impact the acidity of coordinated methane C–H bond. Both density functional theory – for geometry optimization – and highly accurate DLPNO-CCSD(T)/def2-QZVPP /SMD-DMSO simulations – were employed for energetics calculations. The present research indicates that both the supporting ligand *and* the identity of the metal have a significant impact on the pK_a, with coordinated methane pK_a values ranging from -21.8 (AlH_3-Mn^I) to 6.8 (OH_2-Mn^I) – a remarkable difference of 28.6 pK_a units, **Table 2**. Furthermore, the metal and ligand identity also have a significant impact on the activation barrier with a 34.8 kcal/mol difference between the lowest and highest values (12.1 – 46.9 kcal/mol for AlH_3-Co^+ and PH_3-Mn^+, respectively), **Table 1**. Most importantly, a direct relationship between the pK_a of coordinated methane and the free energy activation barrier was established, **Figure 7**; specifically, enhancement of the Brønsted acidity of a methane C–H bond upon coordination to the L-M^+ complex was found to correlate with lower barriers to activation of methane.

Certain metals and ligands were clearly more favorable than others in enhancing methane activation. The study indicated that the $[Co\text{-}AlH_3]^+$ complex had the highest catalytic potential due to its low activation barrier of 12.1 kcal/mol and high acidity of ligated methane at -21.6 pK_a units, **Table 1** and **Table 2**. Interestingly, barriers tended to be lower for ligands that were Lewis acids such as AlH_3 and BH_3 as well as π-acids such as CO and CNH, **Table 3**. In light of the correlation between the lower pK_a of the ligated methane and the lower free energy barrier of methane activation, it is hypothesized that such ligands yield a more electron deficient metal, which in turn enhances the acidity of the ligated methane C–H bonds. Moreover, one may argue that Z-type ligands deserve additional experimental scrutiny as supporting ligands for methane functionalization catalysis.

While both metals and ligands tested in this study affected the acidity of coordinated methane and hence the kinetic favorability of the subsequent methane activation reaction, ligands displayed a slightly wider range of variation, **Table 3** and **Table 4**. The highest and lowest average ligand $\Delta G^‡$ differed by 12.3 kcal/mol from 17.7 kcal/mol (AlH_3) to 30.0 kcal/mol (PH_3), **Table 4**. This can be compared to the 9.4 kcal/mol difference in $\Delta G^‡$ between the extreme averages for the metals modeled, which ranged from 19.5 kcal/mol (Co^I) to 28.9 kcal/mol (Ni^I), **Table 4**.

Analysis of the individual impacts of the ligands and metals also revealed promising results. Among all metals investigated, LCo^+ complexes were found to have the lowest free energy barriers, with an average of 19.5 ± 4.4 kcal/mol, indicating that cobalt complexes are the most energetically favorable among the models studied for methane activation, **Table 4**. The pK_a values corresponding to the cobalt complexes were the most acidic overall, with an average pK_a of -12.3 pK_a units, **Table 4**. Thus, the cobalt complexes again illustrate the strong positive correlation observed between increased acidity of the coordinated methane C–H bonds and lowered kinetic activation barriers, **Figure 7**.

Among the studied ligands, AlH_3 complexes were shown to have the lowest pK_a of all metal-ligand pairs, with an average pK_a of -18.7 pK_a units, **Table 3**. In addition, AlH_3 also had the lowest free energy barrier among the ligands studied, with an average of 17.7 kcal/mol, **Table 3**. However, there were two exceptions: the AlH_3-Cu^I and AlH_3-Mn^I complexes. As discussed above, Group 13/Cu^I, as well as several Mn^I complexes, were found to be outliers in the methane pK_a vs. $\Delta G^‡$ correlation (**Figure 7**, data points highlighted in red), implying that additional factors other than the acidity of the coordinated methane may determine the actual activation barrier. Some potential factors include the thermodynamic stability of the intermediate generated by methane activation, metal spin state, and

the location of the supporting ligand in either the inner or outer coordination sphere of the metal.

In future studies, solvents other than DMSO could also be modeled. Another area of future interest is the testing of additional ligands. In this study, only nine simple ligands were probed for thermodynamic relationships in methane deprotonation. To test the theory derived from this study, more complex ligands with properties similar to the promising Z-type ligands such AlH_3 and BH_3 and π-acids such as CO and CNH could be investigated to create more industrially practical catalyst leads. Finally, future work should focus on the impact of the metal's formal oxidation state on methane activation barriers. This has been indicated to be a promising avenue for future research given the correlation between methane acidity and methane activation barriers and is currently under investigation in our group.

Supporting Information

Calculated pK_a values of predicted ground state ligand-3d metal methane adducts along with data on the free energy change values (kcal/mol) of the complexes (PDF). Cartesian coordinates for the B3LYP/6-31+G(d)/SMD-DMSO optimized geometries that the CCSD(T)/def2-QZVPP/SMD-DMSO single point energies were calculated from (XYZ).

Acknowledgements

The authors thank the National Science Foundation for their generous support through grant CHE-1464943, and their support of the UNT CASCaM HPC cluster via grant CHE-1531468.

AUTHOR INFORMATION

Corresponding Author

*E-mail: t@unt.edu

Notes

The authors declare no competing financial interests.

References

1() Gunsalus, N. J.; Koppaka, A.; Park, S. H.; Bischof, S. M.; Hashiguchi, B. G.; Periana, R. A. Homogeneous Functionalization of Methane. *Chem. Rev.* **2017**, *117*, 8521–8573.

2() Shilov, A. E.; Shulpin, G. B. Activation of C−H Bonds by Metal Complexes. *Chem. Rev.* **1997**, *97*, 2879–2932.

3() Hu, A.; Guo, J.-J.; Pan, H.; Zuo, Z. Selective Functionalization of Methane, Ethane, and Higher Alkanes by Cerium Photocatalysis. *Science* **2018**, *361*, 668–672.

4() Olah, G. A.; Schlosberg, R. H. Chemistry in Super Acids. I. Hydrogen Exchange and Polycondensation of Methane and Alkanes in FSO3H-SbF5 ("Magic Acid") Solution. Protonation of Alkanes and the Intermediacy of CH5 and Related Hydrocarbon Ions. The High Chemical Reactivity of "Paraffins" in Ionic Solution Reactions. *J. Am. Chem. Soc.* **1968**, *90*, 2726–2727.

5() Streitwieser, A.; Taylor, D. R. Kinetic Acidity of Methane. *J. Am, Chem. Soc. D* **1970**, 1248.

6() Caballero, A.; Despagnet-Ayoub, E.; Diaz-Requejo, M. M.; Diaz-Rodriguez, A.; Gonzalez-Nunez, M. E.; Mello, R.; Munoz, B. K.; Ojo, W.-S.; Asensio, G.; Etienne, M.; Perez, P. J. Silver-Catalyzed C-C Bond Formation Between Methane and Ethyl Diazoacetate in Supercritical CO2. *Science* **2011**, *332*, 835–838.

7(7) Pitsawong, W.; Chenprakhon, P.; Dhammaraj, T.; Medhanavyn, D.; Sucharitakul, J.; Tongsook, C.; van Berkel, W. J. H.; Chaiyen, P.; Miller, A.-F. Tuning of p*Ka* Values Activates Substrates in Flavin-Dependent Aromatic Hydroxylases. *J. Biol. Chem.* **2020**, *295*, 3965–3981.

8(8) Zhou, C. X.; Cundari, T. R. Computational Study of 3d Metals and Their Influence on the Acidity of Methane C–H Bonds. *ACS Omega* **2019**, *4*, 20159–20163.

9() Ho, J.; Coote, M. L. pKa Calculation of Some Biologically Important Carbon Acids -- An Assessment of Contemporary Theoretical Procedures. *J. Chem. Theory Comput.* **2009**, *5*, 295−306.

10() Christman, W. E.; Morrow, T. J.; Arulsamy, N.; Hulley, E. B. Absolute Estimates of $Pd^{II}(\eta^2$-Arene) C–H Acidity. *Organometallics* **2018**, *37*, 2706–2715.

11() Gaussian 16, Revision A.03, M. J. Frisch, G. W. Trucks, H. B. Schlegel, G. E. Scuseria, M. A. Robb, J. R. Cheeseman, G. Scalmani, V. Barone, G. A. Petersson, H. Nakatsuji, X. Li, M. Caricato, A. V. Marenich, J. Bloino, B. G. Janesko, R. Gomperts, B. Mennucci, H. P. Hratchian, J. V. Ortiz, A. F. Izmaylov, J. L. Sonnenberg, D. Williams-Young, F. Ding, F. Lipparini, F. Egidi, J. Goings, B. Peng, A. Petrone, T. Henderson, D. Ranasinghe, V. G. Zakrzewski, J. Gao, N. Rega, G. Zheng, W. Liang, M. Hada, M. Ehara, K. Toyota, R. Fukuda, J. Hasegawa, M. Ishida, T. Nakajima, Y. Honda, O. Kitao, H. Nakai, T. Vreven, K. Throssell, J. A. Montgomery, Jr., J. E. Peralta, . Ogliaro, M. J. Bearpark, J. J. Heyd, E. N. Brothers, K. N. Kudin, V. N. Staroverov, T. A. Keith, R. Kobayashi, J. Normand, K. Raghavachari, A. P. Rendell, J. C. Burant, S. S. Iyengar, J. Tomasi, M. Cossi, J. M. Millam, M. Klene, C. Adamo, R. Cammi, J. W. Ochterski, R. L. Martin, K. Morokuma, O. Farkas, J. B. Foresman, and D. J. Fox, Gaussian, Inc., Wallingford CT, 2016.

12() Neese, F. The ORCA Program System. *WIREs Comput. Mol. Sci.* **2011**, *2*, 73–78.

13() Neese, F. Software Update: the ORCA Program System, Version 4.0. *WIREs Comput. Mol. Sci.* **2017**, *8*, e1327

14() Nazemi, A.; Cundari, T. R. Control of C–H Bond Activation by Mo-Oxo Complexes: pK_a or Bond Dissociation Free Energy (BDFE)? *Inorg. Chem.* **2017**, *56*, 12319–12327.